ACS APPLIED MATERIALS & INTERFACES

Research Article

www.acsami.org

One-Step High-Temperature Solvothermal Synthesis of TiO_2/Sulfide Nanocomposite Spheres and Their Solar Visible-Light Applications

Shangjun Ding,[†,‡] Xin Yin,[†,‡] Xujie Lü,[†] Yaoming Wang,*[,†] Fuqiang Huang,*[,†,§] and Dongyun Wan*[,†]

[†]CAS Key Laboratory of Materials for Energy Conversion, Shanghai Institute of Ceramics, Chinese Academy of Sciences, Shanghai 200050, P.R. China

[‡]Graduate School of the Chinese Academy of Sciences, Beijing 100049, P.R. China

[§]Beijing National Laboratory for Molecular Sciences and State Key Laboratory of Rare Earth Materials Chemistry and Applications, College of Chemistry and Molecular Engineering, Peking University, Beijing 100871, China

Supporting Information

ABSTRACT: A one-step high-temperature hydrated-sulfate assisted solvothermal method has been developed to synthesize TiO_2/sulfide nanocomposite spheres. Different hybrid spheres of TiO_2/CdS, TiO_2/Cu_2S, TiO_2/FeS, TiO_2/Co_9S_8, and TiO_2/ZnS were readily prepared by exploiting different hydrated sulfate. The hydrated sulfate has been proved to play multifunctional roles during the synthetic process, such as spherical template, water supplier, and composition controller. Nanocrystal CdS can be reduced from $CdSO_4$ at a high solvothermal temperature of 350 °C, and the TiO_2/CdS nanocomposite spheres prepared by this method exhibit superior visible-light-driven photocatalytic efficiency because of its effective heterointerface and high crystallinity.

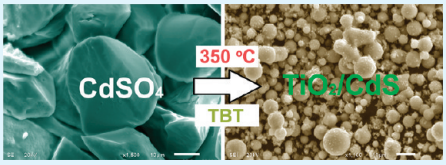

KEYWORDS: *titanium dioxide, nanocomposite, solvothermal method, visible-light photocatalysis, hydrated sulfate*

1. INTRODUCTION

Titanium dioxide (TiO_2) has attracted extensive attention for solar energy applications during the past decades due to its superior physical and chemical properties.[1−7] However, the wide band gap TiO_2 (3.2 eV) can absorb only 5% of the entire solar spectrum, resulting in a poor conversion efficiency in solar applications. Narrow-band gap semiconductor materials have been used to act as light-harvesting sensitizers to enhance the photoelectric properties of TiO_2. Especially, many metal chalcogenide semiconductors (MQ_x: CdS, CdSe, PbS, SnS_2, SnS, Bi_2S_3, In_2S_3, $CuInS_2$, etc.) attract more attention because of their appropriate direct energy band gaps.[8−18]

Such semiconductor heterostructures (or nanocomposite) can compensate the disadvantages of the individual components to induce some synergistic effects, such as efficient charge separation and migration, expanded visible light response, and the improved photostability. Various preparation methods, such as precipitation,[10] chemical bath deposition (CBD),[11,12] microemulsion process,[16] chemical vapor deposition,[17] and electrochemical deposition,[18] have been exploited to construct TiO_2/MQ_x nanocomposite. But all of these synthetic methods are two-step processes, namely, to prepare TiO_2 nanoparticles, nanostructures, or porous films first, and then to anchor nanocrystals or coat a thin layer of sensitizer semiconductors onto the TiO_2 matrix. These two-step processes are usually cumbersome and the heterointerface obtained may not be able to ensure to achieve these targeted advantages. To simply achieve efficient TiO_2/MQ_x interface, the one-step synthesis of the composite can possess in situ built-in connectivity between TiO_2 and MQ_x to favor the charge transfer.

Recently, we proposed the hydrated-sulfate assisted solvothermal (HAS) strategy to prepare TiO_2/metal oxide (MO_x: ZnO, Fe_2O_3, Co_2O_3, etc.) heterostructures with an excellent heterointerface for charge separation.[19] The hydrated-sulfate was introduced to concurrently serve as template and reactant to fabricate composite oxides during a facile one-step process, and those composites exhibited an enhanced ability of charge transfer. In the present study, our HAS method was further expanded to solvothermally synthesize TiO_2/metal-sulfide (MS_x, x depends on M) nanocomposite by rising the reaction temperature up to 350 °C. The reductive agent produced at high temperature can reduce metal sulfate into MS_x, which was in situ integrated into the TiO_2 matrix to form nanoparticle-assembled composite spheres. By exploiting different hydrated sulfate, diverse TiO_2/MS_x nanocomposite spheres, such as TiO_2/CdS, TiO_2/Cu_2S, TiO_2/Co_9S_8, TiO_2/FeS, and TiO_2/ZnS, were readily prepared. Especially, the TiO_2/CdS hybrid sample exhibits superior visible-light-driven photocatalysis due to its effective heterointerface and high crystallinity.

2. EXPERIMENTAL SECTION

All the chemicals were commercially purchased and used without further purification. In a typical experiment for preparing TiO_2/sulfide hybrid spheres, hydrated metal sulfate ($ZnSO_4{\cdot}7H_2O$, $CuSO_4{\cdot}5H_2O$, $CoSO_4{\cdot}7H_2O$, $FeSO_4{\cdot}7H_2O$, $CdSO_4{\cdot}8/3H_2O$, 1.2 mmol) was added into absolute ethanol (20 mL) under continuously stirring for 4 h to

Received: September 30, 2011
Accepted: December 15, 2011
Published: December 15, 2011

form a white suspension, and then tetrabutyl titanate (TBT, 4 mL) was introduced. The slurry was stirred for another 1 h, transferred to a quartz-lined autoclave (7 mL) and reacted at 350 °C for 20 h. The resultant precipitate was washed thoroughly with ethanol and deionized water three times and dried at 80 °C for 12 h.

The crystal structure and phase identification of the samples were performed by X-ray diffraction (XRD Bruker D8 ADVANCE) with a monochromatized source of Cu $K_{\alpha 1}$ radiation (λ = 0.15405 nm) at 1.6 kW (40 KV, 40 mA). A JEOL JSM-6510 scanning electron microscope (SEM), equipped with an energy-dispersive analytical-X-ray spectroscopy (EDS Oxford INCA Model 6498), was used to investigate the morphologies and chemical compositions of the samples. Field-emission transmission electron microscopy (TEM) observations as well as high-resolution transmission electron microscopy (HRTEM) images were collected on a JEOL JEM 2100F microscope working at 200 kV. The optical absorption characteristics were determined via UV−vis diffuse reflectance spectrum (DRS) on a spectrophotometer (Hitachi U4100). Nitrogen adsorption−desorption isotherms at 77 K were measured on a Micrometitics Tristar 3000 system. The pore size distributions were calculated from desorption branches of isotherms by the Barrett−Joyner−Halenda (BJH) method. X-ray photoelectron spectroscopy (XPS) measurements were performed on a Thermo Scientific ESCALAB 250 spectrometer with a monochromized Al K_{α} X-ray resource (1486.6 eV).

The photocatalytic activities of the composite spheres were evaluated by the photodegradation of a model pollutant methylene blue (MB) under visible-light. A 500 W Xe lamp with a 420 nm cutoff filter was used as the light sources. The experiments were performed as follows: 150 mg photocatalysts was added into 150 mL MB solution (2 mg L^{-1}). Before illumination, the suspension was magnetically stirred for 1 h in the dark to reach the adsorption−desorption equilibrium between the MB and the photocatalysts. Then the suspension was stirred and exposed to light irradiation. The concentrations of the MB were monitored by checking the absorbance at 664 nm during the degradation process by using a Hitachi U-3010 UV−vis spectrophotometer.

3. RESULTS AND DISCUSSION

3.1. Morphology and Microstructure of TiO_2/CdS Nanocomposite spheres. The reaction temperature plays a crucial role on fabricating TiO_2/MS_x nanocomposite spheres via the hydrated-sulfate assisted solvothermal (HAS) method. Taking the one-step preparation of TiO_2/CdS composite with the assistance of hydrated cadmium sulfate ($CdSO_4{\cdot}8/3H_2O$) as a typical example, two reaction temperatures (240 and 350 °C) were selected for comparison. At the high solvothermal temperature (350 °C), well-developed composite spheres with diameters range from 1 to 10 μm were readily prepared (Figure 1a) and these spheres are all assembled by nanoparticles (Figure S1 in the Supporting Information). The TiO_2/CdS composite phases were verified by the XRD patterns (Figure 1b). The strong main diffraction peaks can be assigned to the well-crystallized anatase TiO_2 (JCPDS Card No. 21−1272), and the crystallite size of TiO_2 is calculated to be ~16 nm according to the Scherrer equation. Additional peaks at 26.5, 28.2, 43.8, and 51.9° are attributed to the hexagonal phase of CdS (JCPDS Card No. 65−3414).

The TiO_2/CdS composite nature is further evidenced by UV−vis spectra (Figure 1c). The pure TiO_2 only absorbs in UV region with a band edge of approximately 400 nm (E_g = 3.2 eV). But the composite sample exhibits two absorption edges corresponding to TiO_2 (at 400 nm) and CdS (at 550 nm), with strong absorbance in the visible-light region. It is in accordance with the bright yellow color of the as-prepared powder (inset of Figure S1). From the plot of Kubelka−Munk Function ($F(R)=(1-2R)^2/2R = \alpha/S$) versus the photon energy, the band gap of

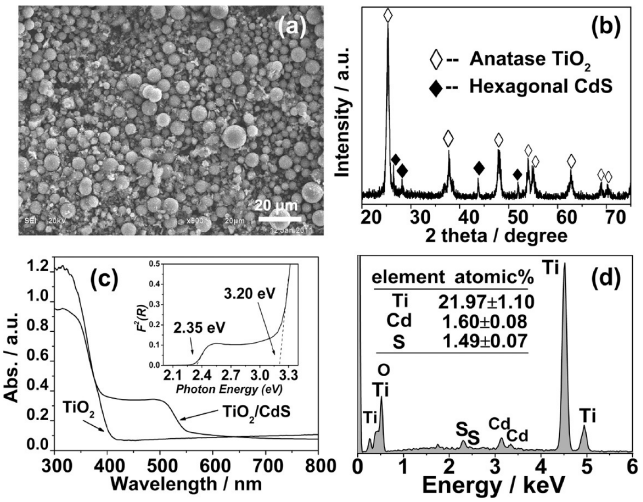

Figure 1. (a) SEM morphology, (b) XRD pattern, (c) UV−vis absorption spectrum, and (d) EDS profile of the as-prepared TiO_2/CdS nanocomposite spheres through the high-temperature HAS method at 350 °C.

CdS was estimated to be 2.35 eV (inset of Figure 1c). The respective Cd and S contents in the composite spheres were determined to be 7.3 and 6.8 at. % from the EDS analyses (Figure 1d). The element mole ratio of Cd:S is close to 1:1.

But for the low-temperature (240 °C) reaction, TiO_2/CdS nanocomposite spheres can not be obtained. Instead, the as-prepared TiO_2 spherical particles possess poor crystallinity and small crystallite size (~7 nm calculated from XRD), as shown in Figure S2a-b. The UV−vis diffuse reflectance spectrum shows an additional absorption shoulder in the visible-light range (Figure S2c), consistent with the pale pink sample color (inset of Figure S2c). Only a tiny trace of Cd (<0.5 at. %) in the as-prepared TiO_2 spheres was detected from the EDS measurement (Figure S2d), which may be due to the little CdO phase or the Cd-doping. Therefore, it reveals that low-temperature solvothermal reaction (e.g., 240 °C, the softening point of polytetrafluoroethylene autoclave linear) does not favor to produce CdS phase.

Detailed crystal structure of the TiO_2/CdS composite sample prepared at 350 °C was further investigated by TEM observations, as show in Figure 2. The wide field of vision shows spherical structure (Figure 2a), and each sphere can be dispersed into nanoparticles by 800 W ultrasonic vibrations (Figure 2b). The hexagonal shaped nanoparticles with the size range from 8 to 40 nm are attributed to CdS nanocrystals, featured by the mean lattice distances of about 3.57 Å (100) and 3.34 Å (002) for hexagonal-CdS phase in the HTEM characterizations (Figure 2c). The closely contacted nanoparticle with d-values of about 3.52 Å indicates anatase TiO_2 and a well-developed heterointerface can be visualized between CdS and TiO_2 nanocrystals (Figure 2c and Figure S3a). In addition, the nanocrystal connective way of one-CdS to multiple-TiO_2 is prevalently observed from HTEM images (Figure 3d and Figure S3b), so we assume that the CdS and TiO_2 nanoparticles are three-dimensional connected with each other in the composite spheres, benefiting the production of more heterointerfaces. Both TiO_2 and CdS nanocrystals have clear lattice fringes, indicating the high reaction temperature (350 °C) is in favor of the high crystallinity.

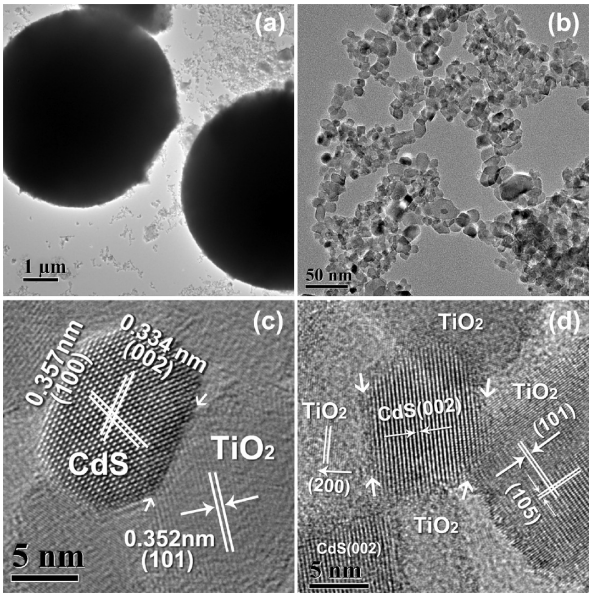

Figure 2. (a) Overall TEM view of solid spheres, (b) TEM picture of the ultrasonic-treated nanoparticles, (c, d) HTEM pictures of CdS, TiO_2 nanocrystals, and the heterointerfaces between them.

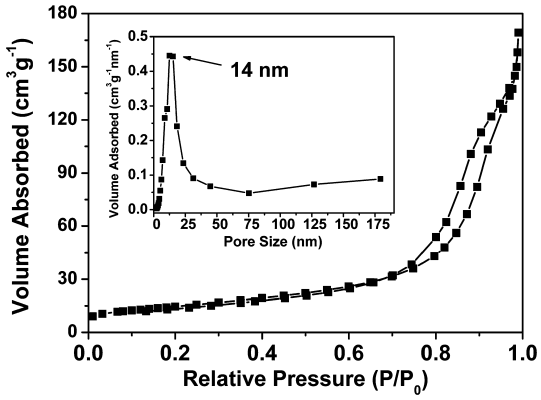

Figure 3. Nitrogen adsorption–desorption isotherm and the corresponding pore size distribution (inset) of the TiO_2/CdS composite sample prepared at 350 °C.

The pore structure of the TiO_2/CdS composite sample was investigated by nitrogen adsorption–desorption isothermals and the pore size distribution was calculated by BJH method according to the desorption branch. As shown in Figure 3, the typical Langmuir IV hysteresis indicates a mesoporous structure and a relative high surface area. The average pore size was determined to be 14 nm and the BET specific surface area of this nanocomposite sample is about 52.39 $m^2\ g^{-1}$.

The surface composition and element valence states of the as-prepared TiO_2/CdS spheres were determined by X-ray photoelectron spectroscopy (XPS) analysis. Figure S4 depicts the XPS survey scan spectrum consisting of Ti, Cd, O, S and traces of contaminated C elements, while the narrow scan spectra of Ti2p, Cd3d, S2p, O1s core levels are shown in Figure 4. Two peaks located at 459.0 and 463.9 eV in Figure 4a correspond to Ti $2p_{3/2}$ and Ti $2p_{1/2}$ of Ti^{4+} in TiO_2, respectively and no obvious Ti^{3+} XPS signal at around 457.0 eV can be detected.[20] Similarly, the O1s XPS spectrum (Figure 4b) shows a narrow peak with a binding energy of 530.4 eV and slight asymmetry, which was attributed to the crystal lattice

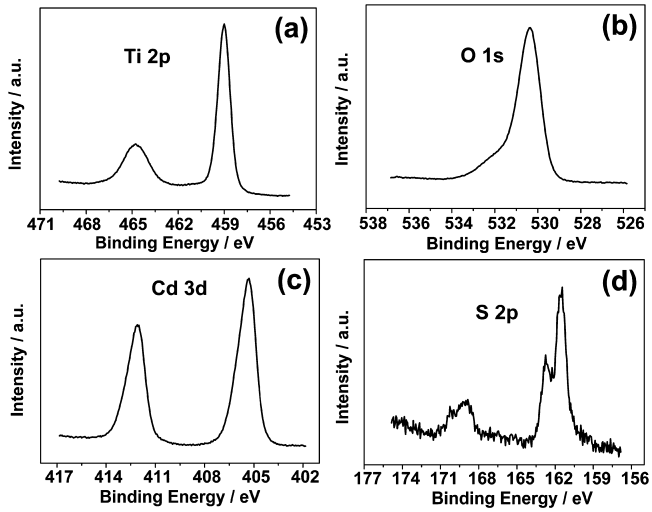

Figure 4. XPS narrow scans for (a) Ti2p, (b) O1s, (c) Cd3d, (d) S2p of the as-prepared TiO_2/CdS composite spheres.

oxygen of Ti–O. The Cd $3d_{5/2}$ and Cd $3d_{3/2}$ peaks (Figure 4c) centered at 405.4 and 412.1 eV with a spin–orbit separation of 6.7 eV are assigned to Cd^{2+} of CdS, consistent with the reported values.[21] Two S2p XPS peaks were also represented in Figure 4d, and the lower bonding energy peak at 161.5 eV is indicative of CdS, while the other peak at 168.8 eV belongs to the more oxidized form of sulfur, such as sulfate (SO_4^{2-}).[22] So a small amount of residual sulfate still existed in the composite spheres, but can not be detected by other measurements. The element content measured by XPS is provided in Table S1 in the Supporting Information, and the atomic ratio of Ti:Cd:S is 22.18: 5.13: 3.50.

3.2. One-Step Growth Mechanism of TiO_2/CdS Nanocomposite Spheres. As reported in our previous HAS method for TiO_2/MO_x composite synthesis,[19] to minimize their surface free energy, irregular hydrated sulfate particles (e.g., $ZnSO_4{\cdot}7H_2O$) can convert into spherical temples when beinh stirred in ethanol, and it contains micro water to hydrolyze the titanium alkoxide to TiO_2 and metal sulfate to metal oxide. The hydrated sulfate plays a multifunctional role (spherical template, water supplier, and composition controller) during the process, which is also applicable to hydrated cadmium sulfate ($CdSO_4{\cdot}8/3H_2O$) in this case.

The template effect of $CdSO_4{\cdot}8/3H_2O$ in absolute ethanol system was investigated carefully in Figure 5a–e, The raw cadmium sulfate particles show large sizes of ~40 μm (Figure 5a), but they gradually dissociated to smaller particles with increasing stirring time in ethanol (Figure 5b–d). In the 4 h stirred suspension, the morphology of cadmium sulfate became near-spherical particles (~1 μm) (Figure 5d). If adding tetrabutyl titanate (TBT) into the suspension and stirring for another 1 h, these particles turned to be smooth spheres, which then can be served as templates for further growth (Figure 5e). The composition was analyzed by EDS (Figure 5f), and the observed Ti, O, Cd, S, C elements indicated that the template sphere may consists of cadmium sulfate and amorphous titanium precursor.

When the suspension was transferred into autoclave and reacted at 350 °C, the TBT is able to self-decompose to TiO_2 in this condition,[23] producing some reductive species such as butyraldehyde (eq 1). In this high-pressure reducing ambient, $CdSO_4$ would be easily reduced to CdS through the possible

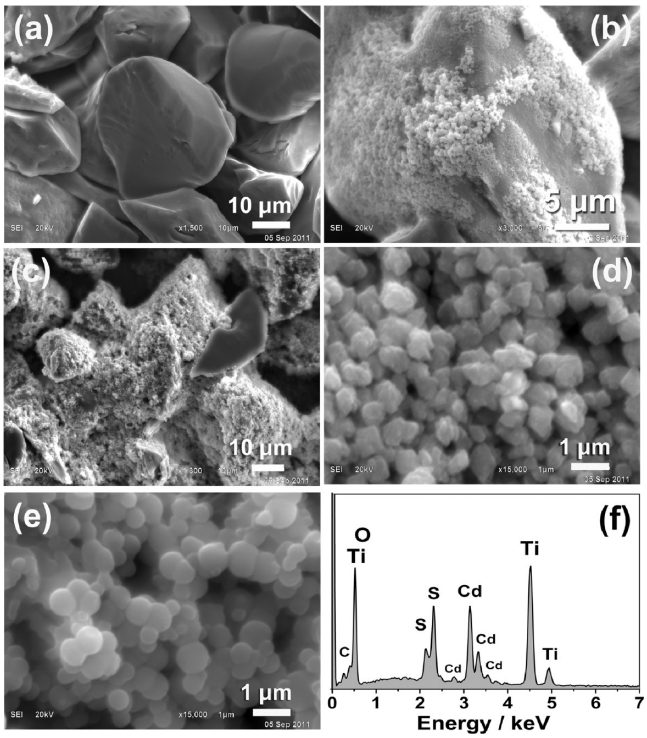

Figure 5. SEM images of (a) the raw $CdSO_4 \cdot 8/3H_2O$ salt, (b–d) the salt stirred in ethanol for (b) 1, (c) 2, and (d) 4 h, and (e) the obtained spherical precursor template by adding TBT into the 4 h-stirred salt in d and stirred for another 1 h. (f) The EDS analysis of the spherical precursor template in e.

reaction in eq 2. If the reaction temperature is not high enough, reducing atmosphere cannot be produced and $CdSO_4$ is unable to convert into CdS. According to this mechanism, the high-temperature HAS (HT-HAS) method has the potential to synthesize other TiO_2/sulfide composite spheres by using different hydrated metal sulfate.

$$Ti(BuO)_4 + 2H_2O \rightarrow TiO_2 + 4C_2H_5CH_2CHO + 4H_2 \quad (1)$$

$$4C_2H_5CH_2CHO + CdSO_4 \rightarrow CdS + 4C_2H_5CH_2COOH \quad (2)$$

3.3. Visible-Light-Driven Photocatalysis Properties of TiO_2/CdS Composite Spheres. The photocatalytic activities of the TiO_2/CdS spherical samples were evaluated by degrading a widely used dye, methylene blue (MB), under visible-light (λ > 420 nm) irradiation. To examine the superiority of HT-HAS method, chemical bath deposition (CBD) process (88 °C) was applied to synthesize TiO_2/CdS composite sample for comparison. Detailed preparation procedure is listed in the Supporting Information. Simply, TiO_2 spheres were first fabricated by HAS method, and then coated a thin layer of CdS through a CBD process using cadmium acetate and thiourea as reactant. The experimental parameters were carefully adjusted according to the amount of hydrated cadmium sulfate used in HT-HAS method, ensuring that the final CdS contents of these two samples are close.

The microstructure of the CBD-TiO_2/CdS composite spheres was also investigated in details. Well-developed spheres with diameters range from 1 to 10 μm are shown in the SEM images (see Figure S5 in the Supporting Information), which is similar to that fabricated by the one-step HT-HAS method. However, the XRD pattern in Figure S6 in the Supporting Information reveals that no obvious CdS peaks can be observed due to its poor crystallinity comparing to the HT-HAS sample. The CBD-TiO_2/CdS composite exhibits the similar absorption edge of CdS, but stronger absorbance in the visible-light region as the UV–vis spectra shown in Figure S7 in the Supporting Information. The average pore size of the CBD-TiO_2/CdS composite spheres was determined to be 17.5 nm by nitrogen adsorption–desorption measurement (see Figure S8 in the Supporting Information) and the BET specific surface area is about 65. 48 m^2g^{-1}, much larger than that of the HT-HAS sample.

TEM characterization (see Figure S9 in the Supporting Information) was further applied to study the crystallinity of CBD-CdS and its heterocontact with TiO_2 matrix. Irregular CdS nanoparticles with size range from 5 to 12 nm are observed coating on the surface of TiO_2 spheres (see Figure S9b in the Supporting Information), and the lattice fringes of 3.37 Å may correspond to the (111) plane of cubic CdS, which is the common phase obtained in CBD method.[24] Figure S9c in the Supporting Information indicates that assembled TiO_2 nanocrystals have similar morphology and crystallinity compared to the HT-HAS sample. However, CdS nanoparticles exhibit poorer crystallinity and the heterointerfaces between CdS and TiO_2 are not as clear as the HT-HAS sample from the HTEM characterization (see Figure S9d in the Supporting Information).

Figure 6a shows the photocatalytic performance of these two TiO_2/CdS composite samples. After visible-light irradiation for

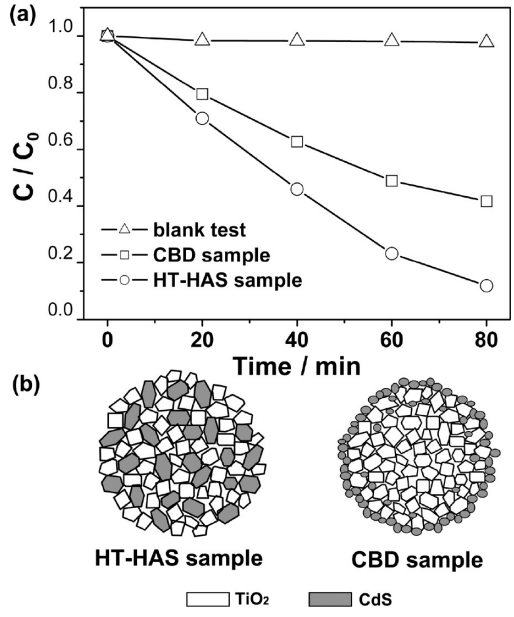

Figure 6. (a) Photocatalytic activities and (b) structure schemes of the two types of TiO_2/CdS composite spheres.

80 min, blank test (MB without any catalyst) exhibits almost no photolysis and MB was almost totally bleached over the HT-HAS-TiO_2/CdS composite spheres, whereas only 55% of MB was photodegraded for the CBD-TiO_2/CdS spheres.

On the basis of the above results and analysis, the robust photochemical performance of the one-step synthesized TiO_2/

dx.doi.org/10.1021/am201343q | ACS Appl. Mater. Interfaces 2012, 4, 306–311

CdS composite is mainly attributed to the high reaction temperature in our HT-HAS method, which benefits the crystallinity improvement of CdS nanocrystals and the formation of well-contacted heterostructures between CdS and TiO_2. The enhanced crystallinity of semiconductors is in favor of charge transport and thus increases the photocatalysis activity,[23,25] whereas the well-developed heterointerface contribute to charge separation.[20] More importantly, from the TEM characterization of HT-HAS sample, TiO_2 and CdS nanoparticles are probably three-dimensional connected with each other as illustrated in Figure 6b, because the reduction of cadmium sulfate template and the TiO_2 generation occurred simultaneously during the one-step HT-HAS process. This is very different from the CBD sample, in which CdS nanoparticles were only coated on the surface of TiO_2 structure as a layer. We deduced that the in situ built-in 3D connectivity between TiO_2 and CdS nanoparticles has a positive influence to the photocatalytic activities, because it can produce more heterointerfaces for efficient charge separation.

3.4. Generality of the HT-HAS Strategy. The synthesis strategy presented here that provides a simple approach for one-step preparation of TiO_2/CdS composite spheres can be widely applied to other systems. For example, $CuSO_4{\cdot}5H_2O$, $CoSO_4{\cdot}7H_2O$, $FeSO_4{\cdot}7H_2O$, and $ZnSO_4{\cdot}7H_2O$ can be introduced instead of $CdSO_4{\cdot}8/3H_2O$, and the corresponding TiO_2/Cu_2S, TiO_2/Co_9S_8, TiO_2/FeS, and TiO_2/ZnS composite spheres were prepared. Figure 7 displays the SEM morphologies of TiO_2 spheres prepared with the assistance of different hydrated metal sulfate. The TiO_2/sulfide composite natures were proved by their XRD patterns in Figure 8. All the samples possess the anatase TiO_2 structure mixed with a small amount of sulfide phase, but their crystallinity was different. The TiO_2/Cu_2S nanocomposite sphere has better crystallinity than others. This may be due to the ionic radii of Ti^{4+} (0.61 Å) is much smaller than Cu^{2+} (0.73 Å), but is very close to Fe^{3+} (0.64 Å) and Co^{3+} (0.61 Å), so Fe^{3+} and Co^{3+} ions are more easily doped into the TiO_2 lattice to induce point defects, decreasing its crystallinity. These composite spheres exhibit significant absorption in visible-light region because of the presence of sulfide phase or some defects, as their UV–vis spectra shown in Figure 9.

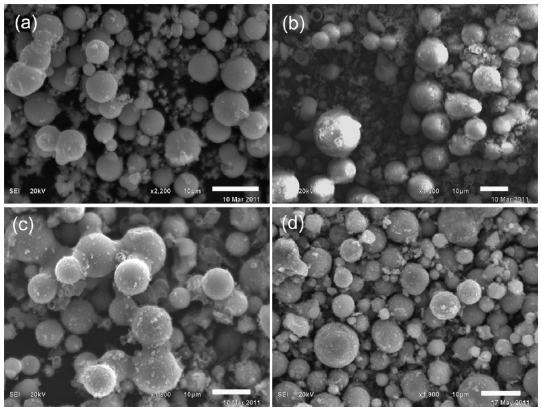

Figure 7. SEM morphologies of TiO_2/sulfide hybrid spheres prepared with (a) $CuSO_4{\cdot}5H_2O$, (b) $FeSO_4{\cdot}7H_2O$, (c) $CoSO_4{\cdot}7H_2O$, and (d) $ZnSO_4{\cdot}7H_2O$ (scale bar: 10 μm).

The hybrid chemical compositions from EDS analysis are listed in Table 1. The element atomic ratio of metal sulfide

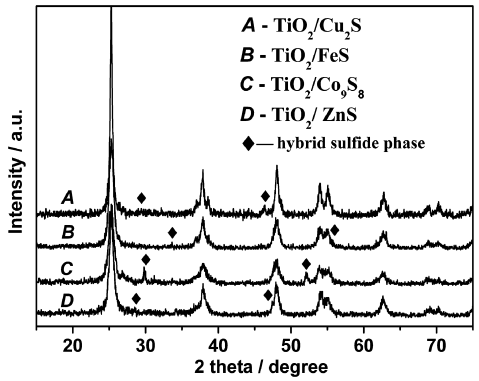

Figure 8. XRD pattern of different TiO_2/sulfide composite spheres.

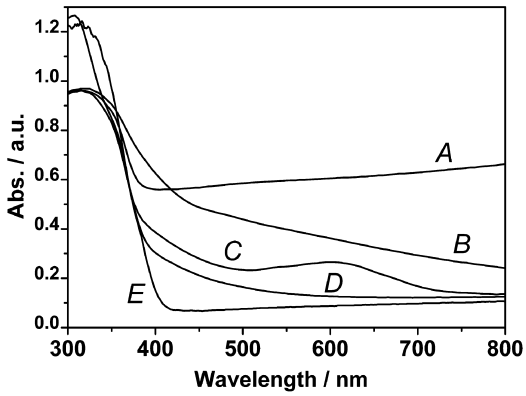

Figure 9. The UV–vis spectra of different TiO_2/sulfide composite spheres: A-TiO_2/Cu_2S, B-TiO_2/FeS, C-TiO_2/Co_9S_8, D-TiO_2/ZnS, E-pure TiO_2.

Table 1. Element Atomic Ratio of Metal Sulfide According to TiO_2 Matrix

	at % in TiO_2 matrix	
TiO_2/MS_x sample	M	S
Ti–Cu–S	1.60 ± 0.08	0.91 ± 0.04
Ti–Fe–S	8.70 ± 0.43	5.87 ± 0.30
Ti–Co–S	13.24 ± 0.66	11.68 ± 0.58
Ti–Zn–S	17.25 ± 0.86	9.41 ± 0.47

(MS_x) was normalized according to the Ti content. In the TiO_2/Cu_2S, TiO_2/Co_9S_8, and TiO_2/FeS samples, the atomic ratio of M:S is very close to the stoichiometric proportion of corresponding metal sulfide (MS_x). But the TiO_2/ZnS composite is an exception, the atomic ratio of Zn:S is near 2:1. In addition, the ionic radii of Zn^{2+} (0.74 Å) is also much larger than that of Ti^{4+} (0.61 Å); however, the TiO_2/ZnS has no better crystallinity than the TiO_2/Cu_2S sample. So we speculate that it is more likely to coproduce a small amount of metal oxide phase (ZnO) in the hydrated zinc sulfate ($ZnSO_4{\cdot}7H_2O$)-assisted method. Meanwhile, Ti^{4+} can be easily doped into the ZnO (or ZnS) lattice to producing some point defects,[3,26] which results in a weak shoulder absorption in the UV–vis spectrum (Figure 9). While the high content of ZnS (ZnO) phase (17.3 at %) in the TiO_2/ZnS composite sample decreases the crystallinity of TiO_2 matrix.

4. CONCLUSION

A high-temperature hydrated-sulfate assisted solvothermal (HT-HAS) method have been developed to prepare TiO_2/

sulfide nanocomposite spheres. TiO_2/CdS, TiO_2/Cu_2S, TiO_2/FeS, TiO_2/Co_9S_8, TiO_2/ZnS were one-step prepared by introducing different hydrated sulfate due to the reductive ambient of 350 °C solvothermal condition. The hybrid sulfide greatly extends the wavelength range of absorbed visible light and the high reaction temperature significantly improves the crystallinity of heterostructures, which make the as-prepared TiO_2/CdS composite spheres exhibit superior visible-light-driven photocatalytic performance over the CBD-derived TiO_2/CdS sample.

■ ASSOCIATED CONTENT

Supporting Information

Chemical bath deposition (CBD) process to prepare TiO_2/CdS composite spheres, SEM, TEM, XRD, XPS, and N_2 adsorption−desorption characterizations of the HT-HAS sample and CBD-sample. This material is available free of charge via the Internet at http://pubs.acs.org.

■ AUTHOR INFORMATION

Corresponding Author

*E-mail: huangfq@mail.sic.ac.cn and huangfq@pek.edu.cn. Tel: +86-21-5241-1620. Fax: +86-21-5241-6360. E-mail: wandy@mail.sic.ac.cn. Tel: +86-21-5241-3214.

■ ACKNOWLEDGMENTS

This work was financially supported by National 973/863 Program of China Grants 2009CB939903 and 2011AA050505, NSF of China Grants 91122034, 50821004, 21101164, 61106088, and Science and Technology Commission of Shanghai Grant 10520706700 & 10JC1415800.

■ REFERENCES

(1) Lü, X. J.; Mou, X. L.; Wu, J. J.; Zhang, D. W.; Zhang, L. L.; Huang, F. Q.; Xu, F. F.; Huang, S. M. *Adv. Funct. Mater.* **2010**, *20*, 509−515.
(2) Ding, S. J.; Huang, F. Q.; Mou, X. L.; Wu, J. J.; Lü, X. J. *J. Mater. Chem.* **2011**, *21*, 4888−4892.
(3) Lü, X. J.; Huang, F. Q.; Mou, X. L.; Wang, Y. M.; Xu, F. F. *Adv. Mater.* **2010**, *22*, 3719−3722.
(4) Palomares, E.; Clifford, J. N.; Haque, S. A.; Lutz, T.; Durrant, J. R. *Chem. Commun.* **2002**, 1464−1465.
(5) Shao, F.; Sun, J.; Gao, L.; Yang, S. W.; Luo, J. Q. *ACS Appl. Mater. Interfaces* **2011**, *3*, 2148−2153.
(6) Sauvage, F.; Chen, D. H.; Comte, P.; Huang, F. Z.; Heiniger, L. P.; Cheng, Y. B.; Caruso, R. A.; Graetzl, M. *ACS Nano* **2010**, *4*, 4420−4425.
(7) Zhang, D. S.; Yoshida, T.; Oekermann, T.; Furuta, K.; Minoura, H. *Adv. Funct. Mater.* **2006**, *16*, 1228−1234.
(8) Sun, W. T.; Yu, Y.; Pan, H. Y.; Gao, X. F.; Chen, Q.; Peng, L. M. *J. Am. Chem. Soc.* **2008**, *130*, 1124−1125.
(9) Lee, Y. L.; Huang, B. M.; Chien, H. T. *Chem. Mater.* **2008**, *20*, 6903−6905.
(10) Peter, L. M.; Riley, D. J.; Tull, E. J.; Wijayantha, K. G. *Chem. Commun.* **2002**, 1030−1031.
(11) Diguna, L. J.; Shen, Q.; Kobayashi, J.; Toyoda, T. *Appl. Phys. Lett.* **2007**, *91*, 023116.
(12) Bessekhouad, Y.; Robert, D.; Weber, J. V. *J. Photochem. Photobiol. A* **2004**, *163*, 569−580.
(13) Ratanatawanate, C.; Xiong, C.; Balkus, K. J. Jr. *ACS Nano* **2008**, *2*, 1682−1688.
(14) Gan, X. Y.; Li, X. M.; Gao, X. D.; Qiu, J. J.; Zhuge, F. W. *Nanotechnology* **2011**, *22*, 305601.
(15) Tsukigase, H.; Suzuki, Y.; Berger, M. H.; Sagawa, T.; Yoshikawa, S. *J. Nanosci. Nanotechnol.* **2011**, *11*, 3215−3221.
(16) Ghows, N.; Entezari, M. H. *Ultrason. Sonochem.* **2011**, *18*, 629−634.
(17) Nanu, M.; Schoonman, J.; Goossens, A. *Adv. Funct. Mater.* **2005**, *15*, 95−100.
(18) Zhu, W.; Liu, X.; Liu, H. Q.; Tong, D. L.; Yang, J. Y.; Peng, J. Y. *J. Am. Chem. Soc.* **2010**, *132*, 12619−12626.
(19) Lü, X. J.; Huang, F. Q.; Wu, J. J.; Ding, S. J.; Xu, F. F. *ACS Appl. Mater. Inter.* **2011**, *3*, 566−572.
(20) Su, C. Y.; Shao, C. L.; Liu, Y. C. *J. Colloid Interface Sci.* **2011**, *359*, 220−227.
(21) Wu, L.; Yu, J. C.; Fu, X. Z. *J. Mol. Catal. A: Chem.* **2006**, *244*, 25−32.
(22) Hota, G.; Idage, S. B.; Khilar, K. C. *Colloids Surf., A* **2007**, *293*, 5−12.
(23) Lü, X. J.; Ding, S. J.; Xie, Y. A.; Huang, F. Q. *Eur. J. Inorg. Chem.* **2011**, 2879−2883.
(24) Patil, S. B.; Singh, A. K. *Appl. Surf. Sci.* **2010**, *256*, 2884−2889.
(25) Biswas, S.; Hossain, M. F.; Takahashi, T.; Kubota, Y.; Fujishima, A. *Thin Solid Films* **2008**, *516*, 7313−7317.
(26) Chung, J. L.; Chen, J. C.; Tseng, C. J. *Appl. Surf. Sci.* **2008**, *255*, 2494−2499.